Eur Biophys J (1997) 26: 227–237

ARTICLE

C. Ober · M. Burkardt · H. Winkler · A. X. Trautwein
A. A. Zharikov · S. F. Fischer · F. Parak

Low temperature study of myoglobin-ligand rebinding kinetics with Mössbauer spectroscopy

Received: 19 November 1996 / Accepted: 17 March 1997

Abstract We have studied the recombination kinetics of carboxymyoglobin (after photodissociation of the CO ligand) by Mössbauer spectroscopy for temperatures in the range 4.2–60 K. The observed kinetics display non-exponential behaviour which was monitored over periods of a few days. It is shown that the time dependence of the kinetics can be reduced to a single universal function of the temperature-dependent variable $(t/\tau_{1/2}(T))^{\beta(T)}$. The half-decay time $\tau_{1/2}(T)$ and the scaling parameter $\beta(T)$ are analysed for the presence of tunneling effects. The non-Arrhenius temperature dependence of the half-decay time below 60 K is interpreted as activated tunneling in models with an Eckart barrier or a fluctuating barrier.

Key words Carbonmonoxy-Myoglobin · Recombination kinetics · Mössbauer spectroscopy · Scaling law · Activated tunneling

1 Introduction

Myoglobin (Mb), the oxygen storage protein in muscle, has become a model system for the study of the relationship between protein structure, protein dynamics and function. The active center of myoglobin, a heme group, is shielded from the solvent by a closely packed protein structure, which forms a kind of pocket, the so-called heme pocket. It is well known from high-resolution X-ray data that the static average structures of ligated and unligated myoglobin do not show any path or binding channel through which an exogenous ligand such as O_2 or CO can migrate from the solvent to its binding site at the heme iron (Takano 1977; Philips 1981; Kuriyan et al. 1986). Therefore, structural fluctuations are suggested to play an important role in ligand binding.

At low temperatures (T <180 K), when the dynamics of protein segments are largely frozen, a ligand which is flashed off by light cannot escape from the heme pocket (compare, e. g., Frauenfelder et al. 1988, Schlichting et al. 1994, Hartmann et al. 1996). Thus, it is possible to focus on the last and possibly rate-limiting binding step, i. e. recombination of the ligand with iron from inside the heme pocket.

In our investigation we have studied this recombination, after photodissociation of MbCO, by means of Mössbauer spectroscopy in the temperature range from 4.2 K to about 60 K. Although the overall protein motion is blocked at these low temperatures, binding of a ligand is accompanied by structural changes within the iron-heme group. In unligated myoglobin the heme is domed towards the iron which lies approximately 0.4 Å out-of-plane. Upon recombination structural reorganization of the heme and its surroundings occur: The distance to the proximal histidine increases, the heme becomes planar and the iron is located in-plane. Rebinding of CO is also accompanied by a spin-transition of the ferrous heme iron from high-spin (S=2) in the unligated form to low-spin (S=0) in MbCO. This spin-transition of the central iron can be easily followed by Mössbauer spectroscopy, which is therefore a precise tool for studying the recombination to MbCO at low temperatures, as long as the reaction is sufficiently slow. The present Mössbauer studies of the recombination reaction complement optical absorption measurements of other groups (Iizuka et al. 1974; Austin et al. 1975; Šrajer et al. 1988) by adding data taken in the low-temperature regime ($4.2\ \mathrm{K} \le T \le 60\ \mathrm{K}$) and over long times ($1\ \mathrm{h} \le t \le 1000\ \mathrm{h}$). The advantage of optical studies lies in the possibility of very short measuring times down to the order of picoseconds whereas a typical Mössbauer spectrum is collected during some hours. On the other hand a Mössbauer experiment easily allows data collection over a period of days to

C. Ober · M. Burkardt · H. Winkler · A. X. Trautwein (✉)
Institut für Physik, Medizinische Universität zu Lübeck,
D-23538 Lübeck, Germany

A. A. Zharikov[1] · S. F. Fischer · F. Parak
Fakultät für Physik, Technische Universität München,
D-85747 Garching, Germany

[1] On leave from Novosibirsk. Permanent address: Institute of Chemical Kinetics and Combustion, Siberian Branch of Russian Academy of Science, 630090 Novosibirsk, Russia

months under very stable conditions. The analysis of the rebinding kinetics in the low temperature regime provides information about tunneling effects.

2 Experimental

Sperm whale myoglobin (swMb) enriched with ^{57}Fe to about 90% was dissolved in a 75% (v/v) glycerol/water solution buffered at pH 6.8 with 0.1 M sodium phosphate. The solution was deoxygenated and reduced with sodium dithionite to give deoxy-Mb. To obtain MbCO the solution was stirred under a CO atmosphere. The resulting protein concentration of the sample was 5 mM. 330 µl of the MbCO solution was confined in a brass cell sandwiched with optically transparent mylar windows, which were made gas-tight using indium-sealed brass covers. A lead washer with an inner diameter of 5 mm selects a homogeneous 3 mm thick part of the sample.

Photolysis of MbCO inside the cryostat was accomplished by using a specially designed sample holder with two sets of 23 LEDs (Siemens LD 121) in an annular arrangement, forming a sandwich with the sample cell. Red light ($\lambda = 630-660$ nm at $T = 298$ K) was used; this achieves deep penetration into the sample because it is far away from the Soret absorption band. Before each photodissociation the sample was kept at 120 K for 10 min to ensure that MbCO has completely recombined. Two experimental protocols were followed: the MbCO was continuously exposed to the LED light for various exposure times (typically of the order of some hours) either at 4.2 K or at the desired temperature before measuring the Mössbauer spectra during recombination in the dark. Mössbauer spectroscopy has the advantage that no more light has to be used to probe the sample; at low temperatures such probing light may also contribute to photodissocation of the sample. A dissociation rate of 0.3 h^{-1} was estimated from the rate at which the photoproducts appear in the Mössbauer spectra at 4.2 K, when recombination is very slow. After about 12 h of exposure to light the fraction of photodissociated states nearly reaches saturation. Because of the competition between photodissociation and rebinding this maximum of photoproducts is temperature dependent (92% at 4.2 K but only 40% at 57.6 K).

The Mössbauer measurements were done in absorption geometry with a drive in constant-acceleration mode and with a 0.5 GBq ^{57}Co(Rh)-source. For variation of sample temperature a flow cryostat (CF500, Oxford Instruments) was used with a temperature stability of ±0.5 K. Only the long-time measurements at 4.2 K were done in a bath cryostat (MD 306, Oxford Instruments). Foils of α-iron with 5 µm or 25 µm thickness were used for velocity calibration; the values of isomer shifts thus refer to α-iron at room temperature. At 4.2 K the Mössbauer spectrum of MbCO shows a quadrupole doublet with isomer shift $\delta_{\alpha-\mathrm{Fe}} = (0.271 \pm 0.008)$ mms^{-1}, quadrupole splitting $\Delta E_Q = (0.336 \pm 0.003)$ mms^{-1} and linewidth $\Gamma_{\mathrm{exp}} = (0.266 \pm 0.005)$ mms^{-1} (see Fig. 1). Owing to the spin transition of the heme iron that accompanies the photodissociation of MbCO the doublet of the low-temperature photoproduct Mb* is easy to separate from that of MbCO: The unligated high-spin state exhibits a larger isomer shift $\delta_{\alpha-\mathrm{Fe}} = (0.893 \pm 0.008)$ mms^{-1} and a much wider quadrupole splitting $\Delta E_Q = (2.340 \pm 0.005)$ mms^{-1} than the ligated low-spin state; the corresponding linewidth is $\Gamma_{\mathrm{exp}} = (0.275 \pm 0.005)$ mms^{-1}. The abbreviation Mb* will be used for the low-temperature photoproduct to denote that the CO is still in the heme pocket in this state and myoglobin may not have relaxed to its stable deoxy-Mb conformation. For comparison the Mössbauer parameters of crystalline deoxy-Mb measured by us at 4.2 K are $\delta_{\alpha-\mathrm{Fe}} = (0.911 \pm 0.006)$ mms^{-1}, $\Delta E_Q = (2.217 \pm 0.002)$ mms^{-1}. This difference between deoxy-Mb and Mb* may be due to different sample preparations (solution versus solid state) as well as to a distinct iron environment in both conformations. A clear answer as to whether or not a special state is created by low-temperature photodissociation cannot be given from the Mössbauer data. The area of the Mössbauer doublets, fitted with Lorentzians, was used to determine the relative intensities of MbCO and the photoproduct Mb*.

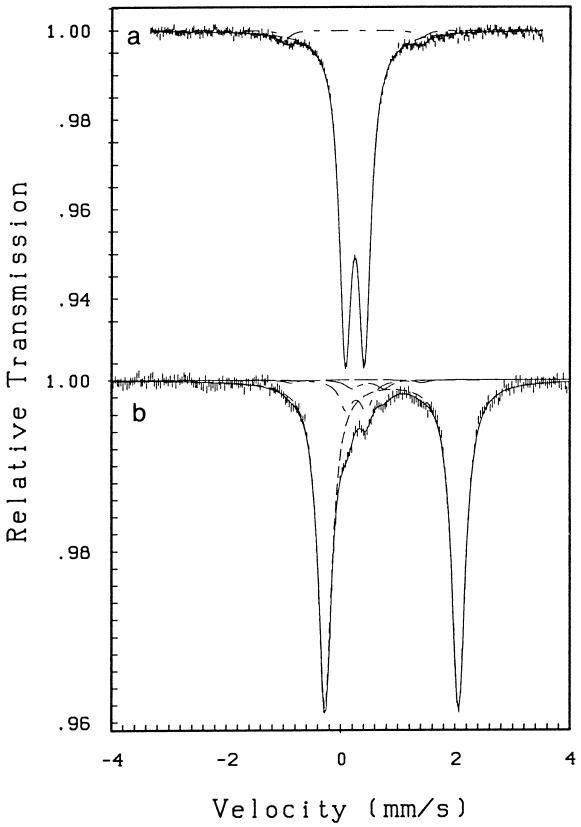

Fig. 1 Mössbauer spectra of (**a**) MbCO and (**b**) the photoproduct Mb* at 4.2 K

3 Scaling law and Mössbauer data

In Fig. 2 we show Mössbauer data on the rebinding for the temperature range 4.2 – 60 K together with the flash-photolysis kinetic data for the temperature range 40 – 120 K (Steinbach et al. 1991[1]). The experimental time window for the Mössbauer study lies between a few hours and 1000 hours. In general the Mössbauer data were obtained after illumination at 4.2 K and subsequent rebinding at the given temperature, except for the data at 47.5 K and 57.6 K, taken from Winkler et al. (1990), where illumination took place at the temperature of the measurement. It is seen from Fig. 2 that the characteristic rebinding times in the Mössbauer experiments are longer than the characteristic rebinding times in the flash-photolysis experiments. For instance, the half-decay times of the kinetics at 40 K measured by Mössbauer spectroscopy and flash-photolysis are about 290 h and 4.5 h respectively. The origin for this relative lengthening of the Mössbauer decay kinetics compared to the optical is not yet completely resolved. There is a difference in the excitation wavelength. The absorption cross-section is much higher for the wavelength used in the optical measurements. This holds in particular for the unbound state. This, as well as the time of illumination has to be considered, when the so called pumping effect is discussed. It is not clear whether the onset of a pumping effect depends only on the fluence, i. e. on the product of absorbance and time of illumination (Nienhaus et al. 1994), if these times get as long as in our experiments. In any case, we will see that our analyses will not depend on this difference, since the time scale can be measured in units of the half decay time.

The observed nonexponential rebinding kinetics in proteins are usually interpreted as the decay of an inhomogeneous ensemble of subsystems with different activation barriers for the rebinding (Austin et al. 1975; Alberding et al. 1976; Agmon and Hopfield 1983; Young and Bowne 1984; Ansari et al. 1987; Frauenfelder et al. 1988; Šrajer et al. 1988, Winkler et al. 1990; Steinbach et al. 1991; Post et al. 1993):

$$n(t,T) = \int e^{-k(H,T)t}\, g(H)\, dH,$$
$$k(H,T) = A \exp(-H/k_B T) \qquad (1)$$

Fitting the experimental data to a static distribution of barriers, $g(H)$, provides a dispersive set of values for H (for review see Frauenfelder et al. 1988).

Another method for the analysis of the kinetic data, even at low temperatures, has been based on the scaling properties of the rebinding. It was found (Zharikov and Fischer 1996 (a, b)) that the rebinding kinetics in myoglobin can be described by a scaling law:

$$n(t,T) = n(x), \quad x = (t/\tau_{1/2})^{\beta} \qquad (2\,\text{a})$$

$$\beta = \frac{T_c}{T^*} \coth(T_c/T) \qquad (2\,\text{b})$$

where $\tau_{1/2}(T)$ is the half-decay time for the rebinding at a given temperature. T_c characterises the onset of tunneling effects and T^* is an upper bound for the temperature at which the kinetics are a completely monotone function of time and can therefore be represented as a decay of some distribution. Within the framework of this analysis no preliminary assumption about the Arrhenius temperature dependence of the rate constant and the choice of a temperature-independent fitting function $g(H)$ was needed.

For the Mössbauer data on the rebinding at 40 K the half-decay time (about 290 h) can be directly extracted from the experiment. Therefore, the scaling properties of these kinetics can be examined without any fitting procedure. In Fig. 3 we demonstrate the scaling behaviour of the flash-photolysis kinetic data and the kinetics measured in the Mössbauer experiment at 40 K. Also shown is the rational approximation for the scaling curve proposed in Zharikov and Fischer (1996 b):

$$n(x) \approx \frac{1}{(1+cx)^{\gamma}}, \quad c = 2^{1/\gamma} - 1 \qquad (3)$$

Note that the multiplier "c" in Eq. (3) is determined by the condition $n(1) = 1/2$.

It is seem from Fig. 3 that the scaling approach can also be applied to the analysis of Mössbauer data.

We used Eqs. (2) and (3) in order to extract the kinetics and to obtain the half-decay times for alle Mössbauer data. In Fig. 4 a the experimental data are fitted according to Eq. (3). The scaling plots of the kinetics are also shown (Fig. 4 b). At very low temperatures the values obtained for the half-decay times are the result of the extrapolation of the behaviour of some part of the kinetics to times longer than the available experimental time. In order to test the quality of such an extrapolation, we have calculated $\tau_{1/2}$ from the rebinding kinetics at 50 K, taken from optical measurements for the time interval between 0.00115 s and

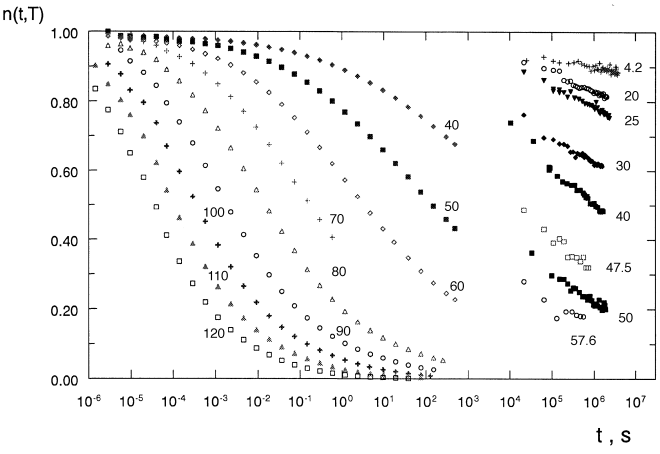

Fig. 2 Low temperature rebinding kinetics in myoglobin. The experimental time window for the Mössbauer data lies in the domain $10^4 - 10^7$ s. The data at 47.5 K and 57.6 K are taken from Winkler et al. (1990). The optical data of the Urbana group (Steinbach et al. 1991) correspond to the time interval shorter than 10^3 s

[1] The data were made available to us by the Urbana group

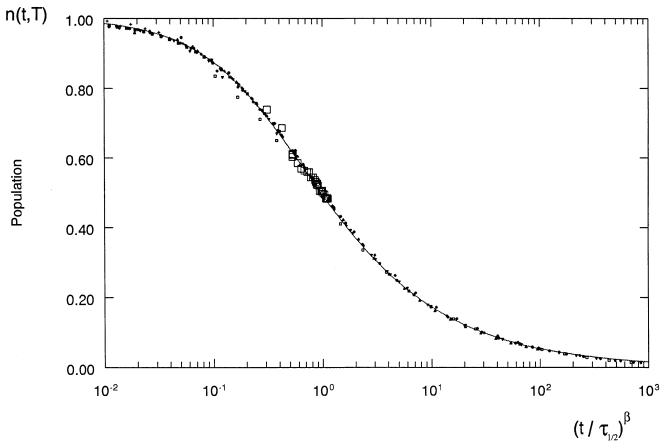

Fig. 3 Scaling plot for the optical kinetics data from Fig. 1. Scaling parameter $\beta(T)$ is calculated from Eq. (2) with $T_c = 30$ K and $T^* = 180$ K. Parameter $\tau_{1/2}(T)$ is the half-decay time for the rebinding at given temperature. *Big squares* correspond to Mössbauer data for the rebinding at 40 K. The *solid line* is the rational approximation, Eq. (3), with $\gamma = 0.51$

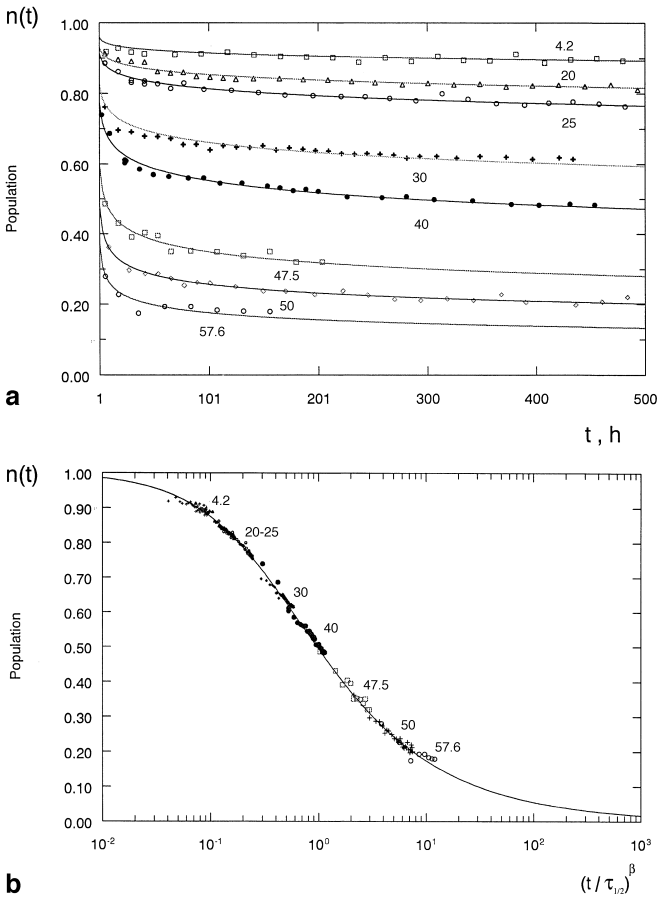

Fig. 4 a, b Mössbauer data on the rebinding of CO in myoglobin. *Solid lines* correspond to the analytical approximation, Eqs. (2) and (3), with $T_c = 30$ K and $T^* = 180$ K. **a** Norm-norm plot. **b** Scaling plot

0.018 s where the population of unbound Mb* changes from 0.96 to 0.915. Note that the full experimental data are available in the range $3 \cdot 10^{-6} - 500$ s where the population of Mb* changes from 1 to 0.43. From the fitting of the kinetics according to Eqs. (2) and (3) we obtained an extrapolation for the half-decay time with $\tau_{1/2}$ about 126 s. This value deviates only slightly from the observed $\tau_{1/2} = 140$ s although the extrapolation was done from a narrow "experimental window" at times about four orders of magnitude shorter than $\tau_{1/2}$.

In addition to the measurements of kinetics we performed a temperature-step experiment. In this experiment the MbCO sample was illuminated for 12 h at 4.2 K. After this time nearly the maximum achievable fraction of the photodissociated states is created. In spite of the slow rebinding rates at 4.2 K we have to expect that about 8% of the photodissociated molecules have rebound during this illumination time and therefore were photodissociated repeatedly. The resulting survival probability can be scanned by a stepwise increase of the temperature to enhance the rebinding. Actually the sample was exposed each time to the corresponding elevated temperature T for 1 h and then the survival probability $N(T, t_0)$ was measured by Mössbauer spectroscopy after quenching to 4.2 K. Following this procedure the temperature was scanned beginning with 10 K in steps of 2.5–5 K up to 85 K. The experimental data are shown in Fig. 5. Owing to the strong temperature dependence of the rebinding rate we assumed that the magnitude of $N(T, t_0)$ at a given temperature is proportional to the population of unbound states $n(t_0, T)$ measured in the kinetic experiments at the same temperature after $t_0 = 1$ h:

$$N(T, t_0) = \frac{N(T = 4.2\ \mathrm{K}, t_0)}{n(t_0, T = 4.2\ \mathrm{K})} \cdot n(t_0, T) = 0.95\, n(t_0, T), \quad t_0 = 1\,\mathrm{h} \tag{4}$$

On the basis of Eqs. (2–4) with $T_c = 30$ K and $T^* = 180$ K one can extract the corresponding half-decay times from the temperature-step experiment. The temperature depen-

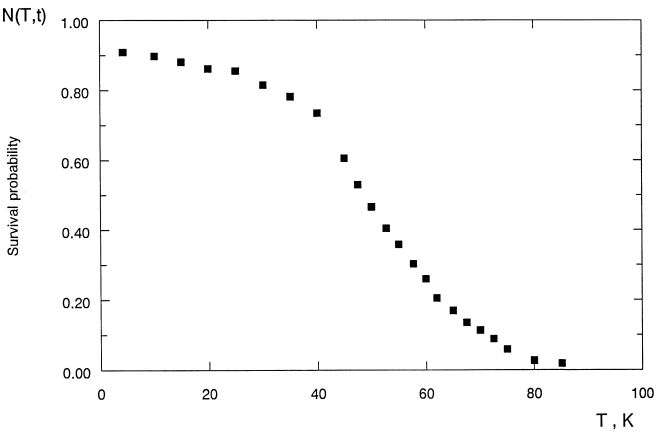

Fig. 5 Survival probability $N(T, t)$ measured with Mössbauer spectroscopy in the temperature-step experiment

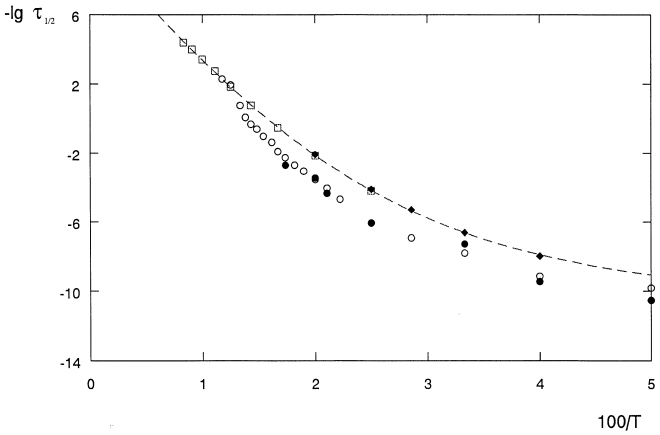

Fig. 6 The Arrhenius plot for the half-decay time, $\tau_{1/2}(T)$. The *full* and *open circles* correspond to Mössbauer kinetic data and the temperature-step experiment, respectively. The *open squares* correspond to the optical data from Fig. 2. The *full diamonds* correspond to the scaling extrapolation of the data from the Fig. 1 a in Steinbach et al. (1991) (For details see the text). The *dashed line* corresponds to the quantum generalization of Eq. (5 a) for $T_c = 35$ K with parameters $A = 10^{10.3}\ s^{-1}$ and $E_a = 13.7$ kJ/mol

dence of the half-decay times obtained in the two types of Mössbauer experiment, as well as by flash-photolysis measurements, is shown in Fig. 6. As one can see, the Mössbauer decay curves give longer half-decay times than the optical data. Also shown is the influence of tunneling, which was fitted in Zharikov and Fischer (1996 b), for the optical data in the range 40 – 120 K to the function

$$-\ln \tau_{1/2} = \ln A - \frac{E_a}{R T_c} \tanh(T_c/T) \tag{5a}$$

$$A \sim 10^{10\pm1}\,s^{-1},\ E_a \sim 13 \pm 1.3\ \text{kJ/mol} \quad \text{for} \quad T_c = 30 \pm 5\ \text{K} \tag{5b}$$

Figure 6 also shows the half-decay times for the optical data at temperatures of 25, 30, 35, 40 and 50 K. These values were derived on the basis of the scaling law according to Eqs. (2) – (3) and experimentally observed times, $t_{0.89}$ at which $n(t_{0.89}, T) = 1/1.12$ holds (see Fig. 1 a in Steinbach et al. 1991). Equation (5 a) describes the data quite well but the way of incorporating the tunneling effects is not unique. Therefore we will elaborate this point further.

4 Tunneling effects

If we model the process as a transition between two wells separated by a barrier, the rate of the transition (or reciprocal decay time) can be determined as

$$\tau^{-1} = k(T) = A \int \rho(E)\, e^{-E/T}\, P(E)\, dE \Big/ \int \rho(E)\, e^{-E/T}\, dE \tag{6}$$

Here $\rho(E)$ is the energy level density in the initially populated wells and $P(E)$ is the tunneling probability. The energy is measured in Kelvin degrees ($k_B = 1$).

We distinguish three regimes corresponding to three different types of temperature dependence for the rate constant: 1) the classical, activated regime, where the over-barrier transitions dominate, 2) the activated tunneling regime, where thermally activated tunneling dominates and 3) the tunneling regime, where only transitions from the lowest energy level without thermal excitation need to be considered (for review see Bell 1980; Hill and Dissado 1982; Goldanski et al. 1989). If the rate constant is measured over a sufficiently wide temperature intervall all three temperature domains can be observed. In the following we shall discuss the main features of the temperature dependence using a quasiclassical formalism in order to classify to observation accordingly.

The quasiclassical approximation for $P(E)$ has the following form:

$$-\ln P(E) = S(E) \approx \frac{2}{\hbar} \int \sqrt{2m(V(x) - E)}\, dx,$$
$$S(E) \geq 1 \quad (E < V_0) \tag{7a}$$

$$P(E) \approx 1, \quad E \geq V_0 \tag{7b}$$

where m is the tunneling mass and V_0 is the barrier height (see Fig. 7). The integration in Eq. (7 a) is performed over the classically forbidden region, $V(x) \geq E$. The variable E in Eqs. (6) and (7) is taken as a continuous variable.

At high temperatures the transitions over the barrier dominate and the temperature dependence of $k(T)$ has an Arrhenius character:

$$k_a(T) \sim \tilde{A}(T) \exp(-E_a/T) \quad \text{with} \quad E_a \approx V_0 \tag{8}$$

The temperature dependence of the preexponential factor is determined by the form of $\rho(E)$. In the case where $\rho(E) \approx \text{const}$ one has $\tilde{A}(T) \approx A$. Qualitatively the temperature range of the Arrhenius behaviour can be determined from the requirement that the integrand in Eq. (6) should be an increasing function of E below the barrier ($E < V_0$):

$$-dS/dE - 1/T \geq 0 \quad \text{or} \quad T > \hbar\omega(E)/2\pi \quad \text{at} \quad E < V_0 \tag{9a}$$

where

$$\hbar\omega(E) = 2\pi[-dS/dE]^{-1} \tag{9b}$$

is the energy level spacing in the inverted barrier. Here and subsequently we assume that $\rho(E) \approx \text{const}$.

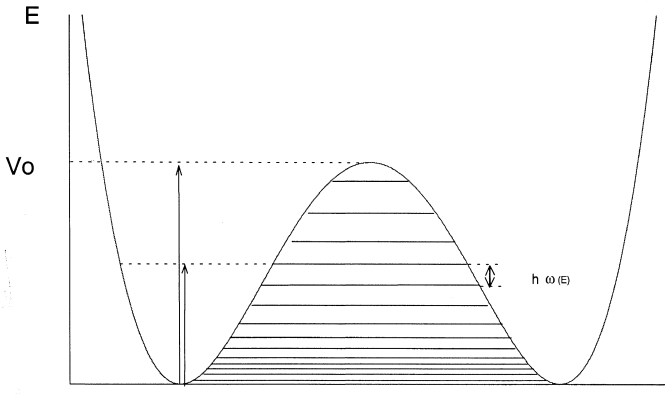

Fig. 7 The model of transitions between wells separated by a barrier. E is the energy of an excited state. V_0 is the barrier height. $\hbar\omega(E)$ is the energy level spacing in the inverted barrier

In the case of a parabolic barrier we have

$$V(x) = V_0 - m\omega_p^2 x^2/2\,, \quad S(E) = 2\pi\,\frac{V_0 - E}{\hbar\omega_p} \tag{10a}$$

$$\omega(E) = \omega_p \tag{10b}$$

The conditions defined in Eqs. (9) and (10) determine a critical temperature T_c

$$T_c = \hbar\omega_p/2\pi \tag{10c}$$

below which under-barrier transitions dominate. For $T < T_c$ the integrand in Eq. (6) is a decreasing function of E and the transition from the bottom of the well determines the rate constant:

$$k_t \sim A e^{-S(0)} = A e^{-V_0/T_c}\,, \quad T < T_c\,, \quad \left(S(0) = 2\pi\,\frac{V_0}{\hbar\omega_p}\right) \tag{11}$$

This limit is known as "quantum plateau" in the temperature dependence of the rate constant. Thus for a parabolic barrier one obtains the functional form

$$k(T) \approx A(T e^{-V_0/T} - T_c\, e^{-V_0/T_c})/(T - T_c) \tag{12}$$

which shows only two temperature domains corresponding to the Arrhenius and temperature-independent laws for the rate constant.

The situation is different if the energy level spacing of the barrier decreases from the top to the bottom of the barrier:

$$\omega_{\min} \le \omega(E) \le \omega_{\max}\,, \quad d\omega/dE = \omega' \ge 0 \tag{13}$$

In this case a temperature domain

$$\frac{\hbar\omega_{\min}}{2\pi} \approx T_c \le T \le T_{ac} \approx \frac{\hbar\omega_{\max}}{2\pi} \tag{14}$$

becomes important, where activated tunneling dominates. Mathematically, this means that the integrand in Eq. (6) has a maximum at energy E^* below the barrier. Estimating the integral, Eq. (6), by the steepest descent method we get:

$$k_{at} \approx A\, f\, e^{-E^*(T)/T - S[E^*(T)]}, \quad \left(f = \frac{\hbar\omega(E^*)}{T\sqrt{\hbar\omega'(E^*)}}\right) \tag{15a}$$

where $E^*(T)$ is defined by the condition

$$\hbar\omega(E^*) = 2\pi T \;\text{ or }\; S'(E^*) + 1/T = 0 \;\; (0 < E^* < V_0) \tag{15b}$$

The energy E^* is the apparent activation energy (Miller 1974)

$$E_{at} = \frac{d\ln(A f/k_{at})}{d1/T} = E^*(T) + [S'(E^*) + 1/T]\, dE^*(T)/dT^{-1} = E^*(T) \tag{16}$$

which decreases from V_0 down to 0 with decreasing temperature in the domain of the activated tunneling.

The apparent activation energy in the "tanh"-law, Eq. (5), is replaced by

$$E_{at} = \frac{E_a}{\cosh^2(T_c/T)} \tag{17}$$

This law can be derived for a model consisting of two symmetrical parabolic wells

$$V(x) = m\omega_0^2\,(|x| - x_p)^2/2\,,$$

$$S(E) = \frac{4V_0}{\hbar\omega_0}\left[\tanh z - \frac{z}{\cosh^2 z}\right] \tag{18a}$$

$$V_0 = m\omega_0^2\, x_p^2/2\,, \quad \cosh z(E) = \sqrt{V_0/E} \tag{18b}$$

Using Eq. (18) in Eqs. (19) and (16) we get:

$$z(E^*) = T_c/T\,, \quad E^* = E_{at} = \frac{E_a}{\cosh^2(T_c/T)} \tag{19a}$$

leading to

$$k_{at} \sim A\exp\left[-\frac{E_a}{T_c}\tanh(T_c/T)\right], \quad E_a = V_0\,,\; T_c = \hbar\omega_0/4 \tag{19b}$$

Qualitatively, Eq. (19) describes the high temperature limit, Eq. (8), as well as "quantum plateau", Eq. (11), at $T \ll T_c$.

The non-Arrhenius behaviour of the rate constant for the activated tunneling regime is pronounced even in the case of the Eckart barrier. One obtains

$$V(x) = \frac{V_0}{\cosh^2(x/a)}\,,$$

$$S_e(E) \approx \frac{2\pi a}{\hbar}\,[(2mV_0)^{1/2} - (2mE)^{1/2}] \tag{20a}$$

$$\omega(E) = \sqrt{\frac{2E}{ma^2}}\,, \quad T_{ac} = \hbar\omega_{\max}/2\pi = \frac{\hbar}{2\pi}\,\sqrt{\frac{2V_0}{ma^2}} \tag{20b}$$

In this model the logarithm of the rate constant is a linear function of T at temperatures below T_{ac}:

$$E^* = BT^2 = V_0\,(T^2/T_{ac}^2)\,, \quad B = V_0/T_{ac}^2 = 2\pi^2\, ma^2/\hbar^2 \tag{21a}$$

$$k_{at} \sim A\exp(-2\sqrt{BV_0} + BT) = A\exp\left[-\frac{V_0}{T_{ac}}\,(2 - T/T_{ac})\right], \quad T \le T_{ac} \tag{21b}$$

This model has been applied for the interpretation of the temperature dependence of the hydrogen abstraction rate in solids (Le Roy et al. 1980; Le Roy 1980; McKinnon and Hurd 1983). In Fig. 8 we compare all three models disscused above with the high-temperature Arrhenius approximation. In order to reproduce the equivalent magnitudes of the rate constant at $T \approx 0$ (see Eqs. [11] [19b] [21b]), we have chosen $T_{ac} = 2\,T_c$ in the case of the Eckart barrier and described the full temperature dependence of the rate constant in this model in accordance with Eqs. (6), (7), (20a), and (21a):

$$k(T) = A e^{-2\sqrt{BV_0}} \cdot [1 + \sqrt{\pi BT}\; e^{BT}\,(\mathrm{erf}\,\sqrt{BT} + \mathrm{erf}\,(\sqrt{V_0/T} - \sqrt{BT}))] \tag{22}$$

where $\mathrm{erf}(z)$ is the probability integral.

It is seen from Fig. 8 that the model with a parabolic barrier displays a very sharp transition from the Arrhenius

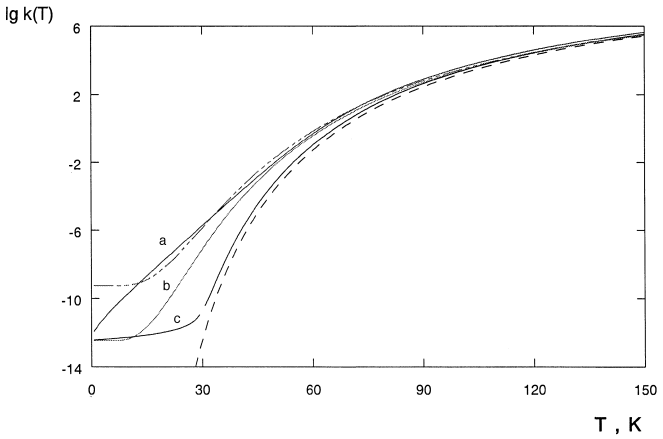

Fig. 8 The temperature dependence of the rate of transitions between wells separated by a barrier. *a* The model with an Eckart barrier, Eq. (22). $T_{ac}=60$ K, *b* The model of parabolic wells, Eq. (19). $T_c=30$ K. *c* The model with a parabolic barrier, Eq. (12). $T_c=30$ K. The *dashed line* corresponds to the Arrhenius approximation, Eq. (8). The *dotted-dashed line* corresponds to the model (*b*) with $T_c=35$ K. The magnitude of the preexponential factor was taken as $A=10^{9.9}$ s^{-1} and the barrier height as $V_0=1550$ K for the all curves

behaviour to the temperature-independent one. The other two models show a wide temperature region of the activated tunneling with a non-Arrhenius rate constant. Changing T_c or T_{ac} (see Fig. 8), one can get a rather close coincidence between both models. The difference exists only in the region of very low temperatures. It should be noted that E^* in the Eckart model can not be less than the lowest energy level, E_0, in the wells. The effects of non-zero E_0 (Le Roy 1980) become important in the case of $2\sqrt{BE_0}\geq 1$ and result in the appearance of the "plateau" behaviour of $k(T)$ at $T\leq\sqrt{E_0/B}$ with zero-temperature constant corrected by the factor $\exp 2\sqrt{BE_0}$.

The phenomenon of activated tunneling has a rather general character and can not be attributed to a specific one-dimensional model only. In complex systems a barrier for the tunneling subsystem can be changed owing to thermal fluctuations of some classical subsystem. In the simplest case one can assume that the tunneling takes place from the lowest energy level with the tunneling probability depending on a coordinate X of the classical subsystem (Trakhtenberg et al. 1982; McKinnon and Hurd 1983; Siebrand et al. 1983; Goldanski 1989)

$$k_q \approx A\, e^{-S(0,X)} \tag{23a}$$

If the fluctuations are fast in comparison to the reaction we have

$$k(T)=\int k_q(X)\ \varphi(X,T)\,dX \Big/ \int \varphi(X,T)\,dX \tag{23b}$$

where $\varphi(X,T)$ is the equilibrium distribution over X.

Using the approximations

$$S(0,X)\approx S(0)-S'X,$$
$$X\leq X_c=S(0)/S' \quad\text{and}\quad S=0,\ X\geq X_c \tag{24a}$$
$$\varphi(X,T)\approx e^{-\gamma X^2/T} \tag{24b}$$

we get

$$k(T)=Ae^{-S(0)+BT}\,[1+\operatorname{erf}(\sqrt{E_a/T}-\sqrt{BT})]/2 + (1/2)\,A\operatorname{erf}\sqrt{E_a/T} \tag{25a}$$

$$B=(S')^2/4\gamma,\quad E_a=\gamma X_c^2=S(0)^2/4B \quad\text{or}\quad S(0)=2\sqrt{BE_a} \tag{25b}$$

The first term in Eq. (25a), corresponding to the activated tunneling, dominates at low temperatures

$$k(T)\approx Ae^{-S(0)+BT}\quad\text{at}\quad T<T_{ac}=\sqrt{E_a/B} \tag{26a}$$

At high temperatures, $T>T_{ac}$, we have an Arrhenius behaviour of the rate constant

$$k(T)=(1/2)\,A\operatorname{erf}\sqrt{E_a/T}\approx A(T/4\pi E_a)^{1/2}\,e^{-E_a/T} \quad\text{for}\quad E_a/T\gg 1 \tag{26b}$$

The activation energy E_a is the energy which is required for the change of the classical coordinate from the equilibrium value $X=0$ to X_c. This energy is not equal to the barrier height of the tunneling subsystem. For example, in the particular case of a modulation of the distance between wells separated by the rectangular barrier one has

$$S(0,X)=(2/\hbar)\sqrt{2mV_0}\,(R-\alpha X),$$
$$B=2mV_0\,\alpha^2/\hbar^2\gamma,\quad E_a=\gamma R^2/\alpha^2 \tag{27}$$

In this case E_a is determined by the equilibrium distance R. It should be noted that the Arrhenius activation energy of the rate constant will be equal to E_a in the case where $V_0>E_a$. If the energy E_a is greater than V_0 the activation energy at high temperatures will be determined by V_0. In this case, in order to describe the transition to the activated regime, one has to use in Eq. (23b) the full expression in Eq. (6) for the rate constant k_q rather than the approximation in Eq. (23a).

We applied the model of the Eckart barrier and the X-model discussed above for the interpretation of the temperature dependence of the half-decay time (see Fig. 9). Both models describe the experimental data quite well and give, for the optical data, approximately the same set of parameters:

$$A\approx 10^{9.8}\ \text{s}^{-1},\quad B\approx 0.48\ \text{K}^{-1},$$
$$V_0\approx 1550\ \text{K}\ \ (\sim 13\ \text{kJ/mol})\ \text{(Eckart)} \tag{28a}$$

$$A\approx 10^{11.2}\ \text{s}^{-1},\quad B\approx 0.51\ \text{K}^{-1},$$
$$E_a\approx 1540\ \text{K}\ \ \text{(X-model)} \tag{28b}$$

At high temperatures the difference between preexponential factors becomes negligible owing to the additional multiplier in the X-model (see Eq. [25b]). The activated tunneling dominates at temperatures $T<T_{ac}\sim 60$ K. In this region we observe the linear temperature dependence of $\log\tau_{1/2}$. The effect of lengthening of the half-decay times measured in the Mössbauer experiments can be attributed to the approximately ten-fold decrease of the preexponential factor or to the increase of the activation energy E_a up to 1700 K (14.1 kJ/mol). The second assumption seems to

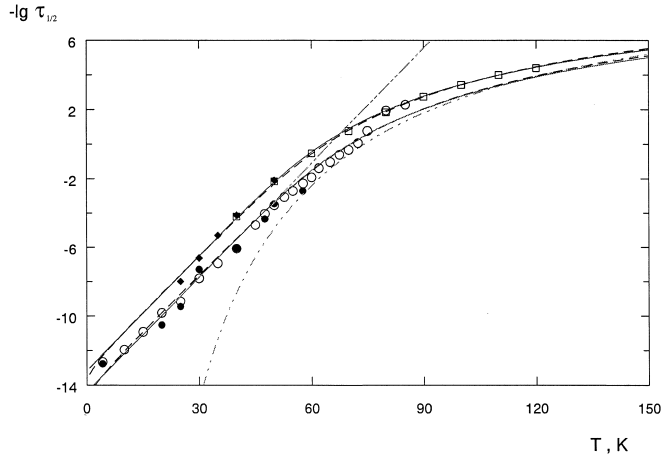

Fig. 9 Log-norm plot for the temperature dependence of the half-decay time. The symbols for the experimental data are the same as in Fig. 6. *Solid lines* correspond to the X-model, Eq. (25), with $A=10^{11.2}$ s^{-1}, $B=0.51$ K^{-1} and activation energies: *a* $E_a=1540$ K, *b* $E_a=1700$ K. The *dashed lines* correspond to the Eckart barrier model, Eq. (22), with $A=10^{9.8}$ s^{-1}, $B=0.48$ K^{-1} and activation energies: *a* $E_a=1550$ K, *b* $E_a=1700$ K. The *dashed-dotted lines* correspond to the linear and Arrhenius approximation (26) in the X-model

be physically more reasonable. For example, in the X-model it is sufficient to assume a 5%-increase of the distance R between wells (see Eq. [27]) in the course of a long illumination in order to explain the observed effect.

5 Scaling kinetics and static distributions

It is known that only a completely monotone function of time which has the property

$$(-1)^l \frac{d^m}{dt^m} n(t) \geq 0 \quad \text{for all } m \tag{29}$$

can be represented as a static decay of an ensemble with a positive distribution over relaxation times (or rate constants). The scaling kinetics of Eqs. (2) and (3) provide a completely monotone function of time only for temperatures $T \leq T^*$ where the scaling parameter $\beta(T)$ is less than unity. Therefore the rebinding can be described for $T \leq T^*$ as a static decay

$$\frac{1}{(1+c(t/\tau_{1/2})^{\beta})^{\gamma}} = \int_0^{\infty} e^{-kt}\, \tilde{g}_r(k,T)\, dk \tag{30a}$$

$$\tilde{g}_r(k,T) = \frac{\beta(T)}{k} \cdot \sum_{n=0}^{\infty} (-1)^n \frac{\Gamma(1+\gamma+n)}{\Gamma(\gamma)\,\Gamma(1+n)} \frac{[(k\tau_{1/2})^{\beta}/c]^{(\gamma+n)}}{\Gamma(1+\beta(T)\,\gamma+\beta(T)\,n)} \tag{30b}$$

with the positive distribution $\tilde{g}_r(k, T)$.

At $T \geq T^* \sim 180$ K ($\beta(T) > 1$) the kinetics, Eq. (30a), form a non-completely monotone function of time. Its second derivative is negative at short times and does not satisfy the condition of Eq. (29). For $T \geq T^* \sim 180$ K the function $\tilde{g}_r(k)$ has negative parts and cannot be considered as a distribution. This means that at the critical temperature $T^* = 180$ K the static interpretation of the rebinding breaks down. The existence of such a critical temperature is a direct consequence of the observed scaling properties, Eqs. (2) and (3), of the rebinding kinetics. On the other hand, if the kinetics were described by a power law

$$n_p(t) = \frac{1}{[1+t/\tau(T)]^{\beta(T)}} \tag{31}$$

such a critical temperature would not follow and the kinetics, Eq. (31), could be represented as static kinetics for all T. The observation of T^* clearly supports the scaling kinetics and not Eq. (31).

The distribution function $g_r(H, T)$ can be derived from $\tilde{g}_r(k, T)$, Eq. (30b) via

$$g_r(H,T) = \tilde{g}_r(k(H,T),T) \left| \frac{\partial k(H,T)}{\partial H} \right| \tag{32}$$

In the high temperature limit of classical activation

$$1/\tau_{1/2} = A \exp(-E_a/T), \quad \beta(T) \approx T/T^* \tag{33a}$$

$$k(H,T) = A \exp(-H/T) \tag{33b}$$

it can be represented as

$$g_r(H,T) = \frac{1}{RT^*} \cdot \sum_{n=0}^{\infty} (-1)^n \frac{\Gamma(1+\gamma+n)}{\Gamma(\gamma)\,\Gamma(1+n)} \frac{(w(H)/c)^{(\gamma+n)}}{\Gamma(1+\beta(T)\,\gamma+\beta(T)\,n)} \tag{34a}$$

$$w(H) = (k\tau_{1/2})^{\beta} = \exp[-(H-E_a)/RT^*], \quad \gamma = 0.51,\ c \approx 3 \tag{34b}$$

As limiting forms we get the following analytical results for $\beta = 1$, or $T = T^*$

$$g_r^*(H) = g_r(H,T^*) = (c^{\gamma}\, RT^*\, \Gamma(\gamma))^{-1} \cdot \exp\left[-\frac{\gamma(H-E_a)}{RT^*} - \frac{1}{c}\, e^{-(H-E_a)/RT^*} \right] \tag{35a}$$

and for $\beta = 0$ closely realized by $T \to 0$

$$g_r^0(H) = g_r(H,\beta=0) = \frac{c\gamma\, e^{(H-E_a)/RT^*}}{RT^*(1+c\exp[(H-E_a)/RT^*])^{1+\gamma}} \tag{35b}$$

It can be seen from Fig. 10 that the distribution $g_r(H,T)$ does not vary much at low temperatures. If we want to preserve this property in the tunneling regime we must assume that the function $w(H)$ (see Eq. [34b]) does not change its functional form by going from the activated regime to the tunneling regime. For $T \to 0$ one can infer from Eqs. (19) and (21) that the corresponding quantum temperatures T_c or T_{ac} must be independent of H. This is always the case for two parabolic wells, Eqs. (18) and (19), where T_c is determined by the frequency in these wells. In the Eckart

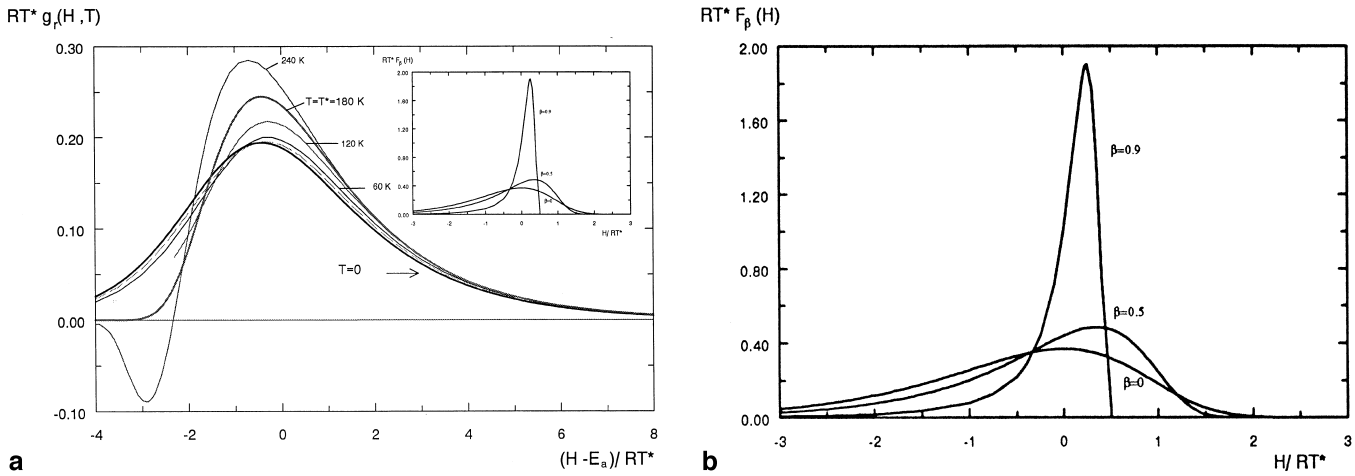

Fig. 10 **a** Distribution function $g_r(H, T)$ for various temperatures evaluated within the Arrhenius limit (*solid lines*). The *dashed line* corresponds to the low-temperature limit for the Eckart model, Eqs. (36 a, b). **b** Temperature variation of the distribution $F_{\beta(T)}(H)$ from the generalized model

model

$$k(H,T) = Ae^{-2\sqrt{B(H)H}}\,[1+\sqrt{\pi B(H)T}\;e^{B(H)T} \cdot (\operatorname{erf}\sqrt{B(H)T} + \operatorname{erf}(\sqrt{H/T} - \sqrt{B(H)T}))] \quad (36\,a)$$

this requirement implies that the parameter B must be proportional to the height of the barrier, H (see Eq. (21 a) and Fig. 10)

$$B(H) = H/T_{ac}^2 \quad (36\,b)$$

The same requirement must also imposed for the X-model.

Apart from the tunneling Fig. 10 shows that the distribution $g_r(H, T)$ varies from $g_r^0(H)$ to $g_r^*(H)$ continuously. At temperatures $T > T^*$ it becomes negative for a certain energy interval and its interpretation as a physical distribution breaks down.

In the following we want to interpret the temperature changes within the framework of a generalized model, where scaling kinetics are represented as a superposition of stretched exponential decays:

$$n(t,T) = \int \exp[-(k(H_1,T)\,t)^{\beta(T)}]\,g_r^*(H_1)\,dH_1,$$
$$k(H_1,T) = A\exp\left(-\frac{H_1}{RT^*\,\beta(T)}\right) \quad (37)$$

In this model the scaling properties are implemented directly in the decay kinetics. The static distribution over the kinetic parameter H_1 is temperature-independent and coincides with the limiting distribution $g^*(H)$ (see Eq. [35 a]). Again we can represent the stretched exponential as a dispersive decay from a distribution $F_{\beta(T)}(H_2)$:

$$n(t,T) = \iint \exp[-(k(H_1+H_2,T)\,t] \cdot F_\beta(H_2)\,g_r^*(H_1)\,dH_1\,dH_2 \quad (38\,a)$$

with

$$F_{\beta(T)}(H) = -\frac{1}{RT^*}\sum_{n=1}^{\infty}(-1)^n\,\frac{\Gamma(1+\beta(T)\,n)}{\Gamma(1+n)} \cdot \exp(nH/RT^*)\,\frac{\sin(\pi\beta(T)\,n)}{\pi\beta(T)} \quad (38\,b)$$

Now the distribution $g_r(H, T)$ is represented as the convolution of the static distribution $g^*(H)$ and the temperature-dependent distribution $F_{\beta(T)}(H)$ which is shown for the particular values of β in the insert of Fig. 10. The temperature variation of $F_{\beta(T)}(H)$ is very reminiscent of a motional narrowing process. It is seen that this distribution narrows with increasing temperature up to a delta function in the limit $\beta \to 1$ (or $T \to T^*$) where the stretched exponential becomes a single exponential:

$$F_{\beta=0}(H) = \frac{1}{RT^*}\exp(H/RT^*)\exp[-\exp(H/RT^*)],$$
$$F_{\beta\to 1}(H) \to \delta(H) \quad (39)$$

6 Discussion

Our application of Mössbauer spectroscopy to the study of rebinding kinetics of unbound CO provided information on tunneling effects. Even though the data showed relatively large scatter, a low temperature tunneling regime for $T < 60$ K could be identified. We applied a recently developed scaling approach which largely simplified the analysis. All data for different temperatures, including those from optical absorption experiments, fall within this scheme on a master curve since they depend only on one scaling parameter $x = (t/\tau_{1/2})^\beta$. The tunneling appears in the exponent β as well as the half decay time $\tau_{1/2}$. Since no clearly pronounced plateau was found at low temperatures, we interpreted this tunneling in terms of activated tunneling and modeled it by an Eckart potential or the so called X-model. Both are best understood within the framework of underlying complex dynamics involving modulations of the barrier by protein fluctuations.

The observation of the scaling up to a critical temperature $T^* \approx 180$ K gives even more support to the conjecture that protein fluctuations play a role in the kinetics below T^*. To clarify this point we would like to summarize the main implications of the scaling approach. In contrast to the models of dispersive kinetics resulting from a static distribution of activation barriers the scaling approach predicts the presence of the critical temperature. This is due to the fact that a survival probability $n(t, T)$, which depends on t and T only via the scaling variable $x=(t/\tau_{1/2}(T))^{\beta(T)}$, fails to remain a completely monotone function for $\beta(T)>1$ so that $\beta(T=T^*)=1$ defines T^*. As a result the rebinding kinetics can not be generated from a superposition of exponentially decaying functions for $T>T^*$. For $T<T^*$ this is possible, but the distributions become temperature dependent. This variation might be due to protein dynamics. A specific distribution may reflect a thermal equilibrium state, which couples to the reactive coordinates of the rebinding process. This view is not in conflict with the hole burning experiments, as long as the protein states fluctuate on a longer time scale than the rebinding scale. We propose that some dynamic aspects should also be incorporated for temperatures $T<T^*$ since the decay kinetics already contain the information on T^*, the temperature at which the fluctuations become critical. We therefore propose to interpret the kinetics in terms of a generalized model, which is capable of separating different parts of the inhomogeneous and homogeneous processes on the temperature dependent time scales of the rebinding kinetics. The static distribution $g^*(H)$ is a critical distribution and relates to the phase transition of the solvent (glycerol). It provides an inhomogeneity sufficient to interpret the kinetic hole burning experiments. In particular it may contain the distribution over slightly differently oriented CO in the unbound state.

The origin of a stretched exponential might be seen in the complex rebinding dynamics of the activated process. The CO can only rebind if the pocket adjusts its shape in order to lower the activation energy. The extended changes in structure between the bound and unbound conformations indicate what kind of fluctuations are needed for the transfer. Considering the many degrees of freedom involved in even a small structural change it becomes evident that not all CO molecules will find the same configuration for an activated complex but all must undergo a dynamic readjustment on the time scale of transfer. As T approaches zero more and more of the local modes freeze out in the dynamic rebinding process and thereby enlarge the width of the effective barrier distribution. In order to prove experimentally that a pure static description is applicable it would be necessary to prepare the unbound system in selective substates and to show that the decay becomes purely exponential. This has not been done yet.

Acknowledgement This work was supported by the Deutsche Forschungsgemeinschaft (SFB 143 and SFB 377) and by an European Union Human Capital and Mobility grant to the MASIMO network (ERBCHRX CT-920072).

References

Agmon N, Hopfield JJ (1983) CO binding to heme proteins: A model for barrier height distributions and slow conformational changes. J Chem Phys 79: 2042 – 2053

Alberding N, Austin RH, Chan SS, Eisenstein L, Frauenfelder H, Gunsalus IC, Nordlund TM (1976) Dynamics of carbon monoxide binding to protoheme. J Chem Phys 65: 4701 – 4711

Ansari A, Berendzen J, Braunstein D, Cowen BR, Frauenfelder H, Hong Kyung M, Iben EIT, Johnson JB, Ormos P, Sauke TB, Scholl R, Schulte A, Steinbach PJ, Vittitow Y, Young RD (1987) Rebinding and relaxation in the myoglobin pocket. Biophys Chem 26: 337 – 355

Austin RH, Beeson KW, Eisenstein L, Frauenfelder H, Gunsalus IC (1975) Dynamics of ligand binding to myoglobin. Biochemistry 14: 5355 – 5373

Bell R (1980) Tunnel effect in chemistry. Chapman and Hall, London, pp 222

Frauenfelder H, Parak F, Young RD (1988) Conformational substates in proteins. Ann Rev Biophys Biophys Chem 17: 451 – 479

Goldanski VI, Trakhtenberg LI, Fleurov VN (1989) Tunneling phenomena in chemical physics. Gordon and Breach Science Publishers, New York London Paris Montreux Tokyo Melbourne, pp 334

Hartmann H, Zinser S, Komnines P, Schneider RT, Nienhaus GU, Parak F (1996) X-ray structure determination of a metastable state of carbonmonoxy myoglobin after photodissociation. Proc Natl Acad Sci USA (in press)

Hill RM, Dissado LA (1982) The temperature dependence of relaxation processes. J Phys C: Solid State Phys 15: 5171 – 5193

Iizuka T, Yamamoto H, Kotani M, Yonetani T (1974) Low temperature photodissociation of hemoproteins: carbon monoxide complex of myoglobin and hemoglobin. Biochim Biophys Acta 371: 126 – 139

Kuriyan J, Wilz S, Karplus M, Petsko GA (1986) X-ray structure and refinement of carbon-monoxy (Fe II)-myoglobin at 1.5 Å resolution. J Mol Biol 192: 133 – 154

Le Roy RJ, Murai H, Williams F (1980) Tunneling model for hydrogen abstraction reactions in low-temperature solids. Applications to reactions in alcohol glasses and acetonitrile crystals. J Am Chem Soc 102: 2325 – 2334

Le Roy RJ (1980) Energy-partitioning tunneling model and prediction of "low" A factor for intramolecular hydrogen transfer reactions. J Phys Chem 84: 3508 – 3516

McKinnon WR, Hur CM (1983) Tunneling and the temperature dependence of hydrogen transfer reactions. J Phys Chem 87: 1283 – 1285

Miller WH (1974) Classical-limit quantum mechanics and the theory of molecular collisions. Adv Chem Phys v XXV: 69 – 177

Nienhaus GU, Mourant JR, Chu K, Frauenfelder H (1994) Ligand binding to heme proteins: the effect of light on ligand binding in myoglobin. Biochemistry 33: 13413 – 13430

Philips SEV (1981) The X-ray structure of deoxy-Mb (pH 8.5) at 1.4 Å resolution. Brookhaven Protein Bank

Post F, Doster W, Karvounis G, Settles M (1993) Structural relaxation and nonexponential kinetics of CO-binding to horse myoglobin. Biophys J 64: 1833 – 1842

Schlichting I, Berendzen J, Phillips GN, jr Sweet RM (1994) Crystal structure of photolysed carbonmonoxy-myoglobin. Nature (London) 371: 808 – 812

Šrajer V, Reinisch L, Champion PM (1988) Protein fluctuations distributed coupling and the binding of ligands to heme proteins. J Am Chem Soc 110: 6656 – 6670

Siebrand W, Wildman TA, Zgierski MZ (1983) Temperature dependence of hydrogen tunneling rate constants. Chem Phys Lett 98: 108 – 112

Steinbach PJ, Ansari A, Berendzen J, Braunstein D, Chu K, Cowen BR, Ehrenstein D, Frauenfelder H, Johnson JB, Lamb DC, Luck S, Mourant JR, Nienhaus GU, Ormos P, Philipp R, Xie A, Young RD (1991) Ligand binding to heme proteins: connection between dynamics and function. Biochemistry 30: 3988 – 4001

Takano T (1977) Structure of myoglobin refined at 2.0 Å resolution. II. Structure of deoxymyoglobin from sperm whale. J Mol Biol 110: 569 – 584

Trakhtenberg LI, Klochikhin VL, Pshezhetskii S Ya (1982) Theory of tunnel transitions of atoms in solids. Chem Phys 69: 121 – 134

Winkler H, Franke M, Trautwein AX, Parak F (1990) Recombination studies of photodissociated MbCO by Mössbauer spectroscopy at low temperatures. Hyperfine Interactions 58: 2405 – 2412

Young RD, Bowne SF (1984) Conformational substates and barrier high distributions in ligand binding to heme proteins. J Chem Phys 81: 3730 – 3737

Zharikov AA, Fischer SF (1996 a) Nonexponential ligand rebinding of CO and O_2 in myoglobin controlled by fluctuations of the protein. Chem Phys Lett 249: 459 – 469

Zharikov AA, Fischer SF (1996 b) Scaling law for nonexponential ligand rebinding of CO in myoglobin. Chem Phys Lett 263: 749 – 758